Multi-Stimuli Responsive Smart Materials: Cyanine Amphiphile Self-Assembly for Photochromic and pH-Switching Applications

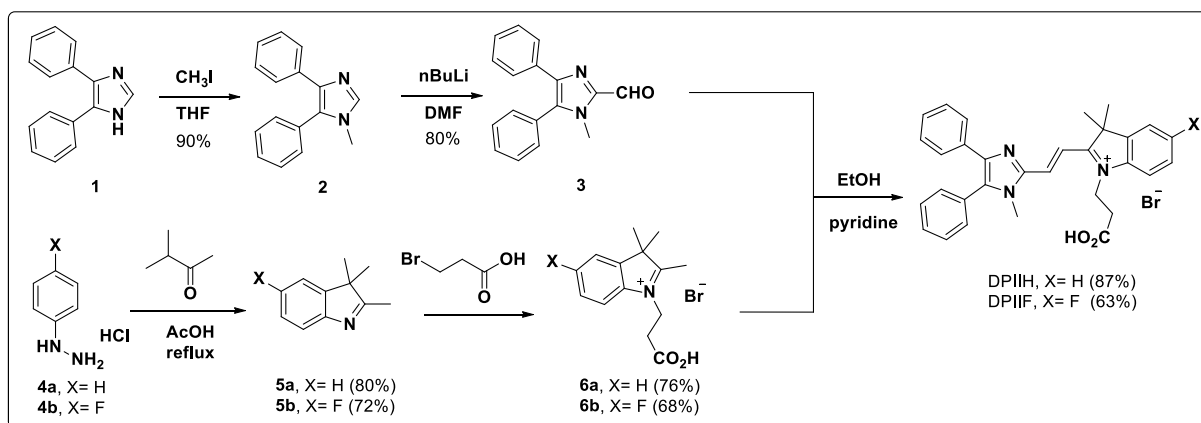Tzu-Yu Tseng,[a,‡] Yao-Chun Yeh,[a,‡] Wei Hsing,[a] Lien-Chen Fu,[a] Mei-Yu Yeh[a,*]

[a]Department of Chemistry, Chung Yuan Christian University, No. 200, Zhongbei Rd., Zhongli Dist., Taoyuan City 320314, Taiwan, Republic of China.

*Corresponding author. E-mail: myyeh@cycu.edu.tw

‡The authors contributed equally to this work.

Scheme S1. Synthetic routes for DPIIH and DPIIF.

Synthesis of 2,3,3-trimethyl-3H-indole (**5a**)

Phenylhydrazine hydrochloride (**4a**) (20.7 mmol, 3.00 g) and 3-methyl-2-butanone (22.8 mmol, 2.44 mL) were dissolved in acetic acid (20mL), then the reaction mixture was refluxed at 120°C for 4h. After cooling to room temperatur, the crude product was extracted with DCM (80mL) and the organic layer was dried over MgSO$_4$ to obtain 2,3,3-trimethyl-3H-indole (**5a**) as a brown liquid (2.63g, 80%). ^{1}H NMR (300 MHz, DMSO-d_6): δ= 1.23 (s, 6H, 2CH$_3$), 2.20 (s, 3H, CH$_3$), 7.14-7.24 (m, 1H, CH), 7.26-7.29 (m, 2H, 2CH), 7.40-7.43 (m, 1H, CH).

Synthesis of 5-fluoro-2,3,3-trimethyl-3H-indole (**5b**)

In a manner similar to that described above, a mixture of (4-fluorophenyl)hydrazine hydrochloride (**4b**) (0.012 mol, 2.00 g) and 3-methyl-2-butanone (0.018 mol, 0.55 mL) were converted to 5-fluoro-2,3,3-trimethyl-3H-indole (**5b**) as a red-brown liquid (1.53 g, 72%). ^{1}H NMR (300 MHz, CDCl$_3$): δ= 1.32 (s, 6H, 2CH$_3$), 2.28 (s, 3H, CH$_3$), 6.97-7.03 (m, 2H, 2CH), 7.44-7.48 (m, 1H, CH).

Synthesis of 1-(2-carboxyethyl)-2,3,3-trimethyl-3*H*-indol-1-ium bromide (IH bromide, **6a**)

2,3,3-trimethyl-3*H*-indole (**5a**) (8.27 mmol, 1.32 g) and 3-bromopropionic acid (10.7 mmol, 1.64 g) were dissolved in dry CH_3CN (5 mL) and the reaction mixture was refluxed under nitrogen for 24h. After cooling to room temperature, the mixture was concentrated under reduced pressure, and diethyl ether was added to precipitate the crude product, followed by purified using chromatography on silica (acetone: diethyl ether 1:2 and DCM) to afford IH bromide (**6a**) as red solid (1.29 g, 76%). ^{1}H NMR (300 MHz, DMSO-d_6): δ= 1.53 (s, 6H, 2CH$_3$), 2.86 (s, 3H, CH$_3$), 2.99 (t, *J*= 9.2 Hz, 2H, CH$_2$), 4.66 (t, *J*= 9.2 Hz, 2H, CH$_2$), 7.61-7.63 (m, 2H, CH), 7.83-7.84 (m, 1H, CH) 7.98-8.00 (m, 1H, CH).

Synthesis of 1-(2-carboxyethyl)-5-fluoro-2,3,3-trimethyl-3*H*-indol-1-ium bromide (IF bromide, **6b**)

In a manner similar to that described above, a reaction mixture of 5-fluoro-2,3,3-trimethyl-3*H*-indole (**5b**) (8.63 mmol, 1.53 g) and 3-bromopropionic acid (9.41 mmol, 1.44 g) were converted to IF bromide (**6b**) as a yellow solid (1.94 g, 68%). ^{1}H NMR (300 MHz, DMSO-d_6): δ= 1.54 (s, 6H, 2CH$_3$), 2.84 (s, 3H, CH$_3$), 2.97 (t, *J*= 9.2 Hz, 2H, CH$_2$), 4.64 (t, *J*= 9.2 Hz, 2H, CH$_2$), 7.46-7.53 (m, 1H, CH), 7.82-7.86 (m, 1H, CH), 8.03-8.08 (m, 1H, CH).

Synthesis of DPIIH

DPI-CHO (1.65 mmol, 0.43 g), IH bromide (1.27 mmol, 0.39 g), and a catalytic amount of pyridine were dissolved in dry ethanol. The reaction mixture was then heated to reflux under nitrogen for 12 hours. After cooling to room temperature, the reaction mixture was concentrated using a rotary evaporator, and the residue was precipitated with diethyl ether to obtain DPIIH as a red-brown solid (0.61 g, 87% yield). ^{1}H NMR (400 MHz, DMSO-d_6): δ= 1.81 (s, 6H, 2CH$_3$), 2.98 (t, *J*= 6.7 Hz, 2H, CH$_2$), 3.77 (s, 3H, CH$_3$), 4.81 (t, *J*= 6.7 Hz, 2H, CH$_2$), 7.25-7.29 (m, 3H, 3CH), 7.44-7.47 (m, 4H, 4CH), 7.58-7.63 (m, 5H, 5CH), 7.86 (d, *J*= 15.6 Hz, 1H, CH), 7.89-7.96 (m, 2H, 2CH), 8.11 (d, *J*= 15.6 Hz, 1H, CH). ^{13}C NMR (100 MHz, DMSO-d_6) δ= 181.7, 172.0, 144.0, 143.3, 142.8, 141.1,

136.9, 136.2, 133.6, 130.9, 129.8, 129.7, 129.4, 128.9, 128.2, 127.3, 123.5, 115.7, 112.5, 52.7, 43.3, 32.7, 32.3, 26.4. HRMS (ESI$^+$) m/z for $C_{31}H_{30}N_3O_2$, calcd 476.2338, found 476.2593.

Synthesis of DPIIF

In a manner similar to that described above, a reaction mixture of DPI-CHO (0.10 mmol, 28 mg), IF bromide (0.10 mmol, 35 mg), and a catalytic amount of pyridine was utilized. This yielded DPIIF as a red-brown solid (0.06 g, 63% yield). ^{1}H NMR (400 MHz, DMSO-d_6): δ= 1.82 (s, 6H, 2CH$_3$), 2.97 (t, J= 6.6 Hz, 2H, CH$_2$), 3.77 (s, 3H, CH$_3$), 4.79 (t, J= 6.6 Hz, 2H, CH$_2$), 7.25-7.30 (m, 3H, 3CH), 7.43-7.50 (m, 4H, 4CH), 7.57-7.59 (m, 4H, 4CH) , 7.83 (d, J=15.1, 1H, CH) , 7.89-7.92 (m, 1H, CH), 8.00-8.03 (m, 1H, CH), 8.09 (d, J=15.1, 1H, CH). ^{13}C NMR (100 MHz, DMSO-d_6): δ= 181.8, 172.0, 161.8, 146.7, 143.3, 142.8, 137.5, 136.9, 133.6, 130.9, 130.1, 129.8, 129.4, 128.8, 128.2, 127.3, 124.3, 116.8, 112.4, 52.9, 43.4, 32.6, 32.2, 26.2. HRMS (ESI$^+$) m/z for $C_{31}H_{29}FN_3O_2$, calcd 494.2238, found 494.2469.

Characterizations

The ^{1}H, ^{13}C, and ^{19}F NMR spectra were captured using a Bruker AVANCE II-400 MHz spectrometer with DMSO-d6 as the solvent, and CF$_3$COOH was utilized as the reference (δ = -75.0 ppm) for the ^{19}F NMR.[S1] Fourier transform infrared (FT-IR) spectra were acquired employing a Thermo Fisher Scientific Nicolet iS5 infrared spectrophotometer to characterize and evaluate the intermolecular and/or intramolecular interactions of DPIIH and DPIIF. Scanning electron microscopy (SEM) using the JEOL JSM-7600F model was utilized to examine the morphologies of DPIIH and DPIIF, with test samples prepared *via* freeze-vacuum drying.[S2] UV-vis absorption and fluorescence emission spectra were recorded with a Shimadzu UV-2550 spectrometer for UV-vis absorption and a Horiba FluoroMax®-4 spectrometer for fluorescence emission. The emission spectra of samples were observed at excitation wavelengths of 495.3 nm, 513.8 nm, and 536.2 nm in water, DMSO, and CHCl$_3$, respectively. To prevent reabsorption of emission from the sample, micro fluorometer cuvettes with a 1 mm light path and 0.35 mL volume were utilized.[S3] Rheological assessments were

performed using a TA rheometer (DHR-1) with a 40 mm parallel plate. The hydrogel sample (400 μL, 1 wt%) underwent an angular frequency sweep test with parameters including a test range of 1-100 rad·s^{-1}, a strain of 1%, 15 points per decade, a sweep mode of "log", and a temperature of 25 °C.[S4]

Biocompatibility of DPIIF

The biocompatibility of DPIIF hydrogel was evaluated by culturing L929 cells with an extraction medium.[S5] The extraction medium was prepared by immersing DPIIF hydrogel in Dulbecco's Modified Eagle Medium (DMEM, Gibco, Life Technologies, Carlsbad, CA, USA) at a volume ratio of 1:10 (hydrogel volume to medium volume) and incubating at 37 °C for two days. L929 cells were seeded in 96-well plates and cultured with DMEM at 37 °C under 5% CO$_2$ for one day. The cells were treated with extraction medium at pH values ranging from 5.5 to 8.0, replacing the DMEM, and allowed to grow for one, three, and five days.[S6,S7] For the light exposure experiment, the selected wells were irradiated with UV light for 30 seconds and subsequently cultured for one, three, and five days.[S8] Cell viability assays were conducted on the L929 cells cultured with the extraction medium and DMEM using the MTT reagent. The optical density of the resulting solution was measured at 595 nm using a BioTek (Winooski, VT, USA) 800 TS microplate reader. Cells that were not exposed to the test hydrogels were assigned to the control group.

Computational methodology

Theoretical calculations were conducted using Gaussian 09 software to elucidate the structural and electronic properties of the molecules under study.[S9] Geometry optimization in both the ground and excited states was achieved *via* density functional theory (DFT) and time-dependent density functional theory (TD-DFT) methods, using the M06-2X density functional with a 6-31G (d,p) basis set, respectively.[S10-S13] The polarizable continuum model (PCM) was employed to simulate the water or DMSO solution environment.[S14] Analysis of frontier molecular orbitals, electrostatic potential

maps, and calculations of both ground and excited states were conducted at the same optimized structural level. Furthermore, UV-Vis absorption and emission spectra of the molecules in water were generated using the TD-DFT method, providing insights into their spectroscopic behavior. Additionally, calculations of ^{1}H NMR chemical shifts (δ), referenced relative to tetramethylsilane (TMS), were performed using the Gauge-Independent Atomic Orbital (GIAO) method developed by Wolinski *et al.*, further enhancing the understanding of molecular properties.[S15] To address the basis set superposition error (BSSE), the counterpoise (CP) method proposed by Boys and Bernardi was employed.[S16] Larger negative binding energy (E_B) values indicate stronger interactions, such as hydrogen bonding, leading to more stable complexes. Moreover, non-covalent interactions were visualized and analyzed in real space using Multiwfn 3.7 software, with graphical representations generated using VMD 1.9.[S17, S18]

Table S1. Physical properties of DPIOH, DPIIH, DPIIF.

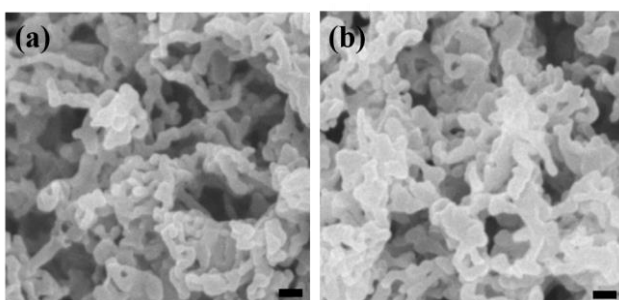|	Conc. (wt%)	Appearance	G′, G″ (Pa)
DPIOH	0.5-2.0	Solution	/
DPIIH	0.5-2.0	Solution	/
DPIIF	0.5	Solution	/
DPIIF	1.0[a]	Gel	688.0, 201.3
DPIIF	2.0	Gel	2387.3, 472.2

[a]The lower critical gelation concentration.

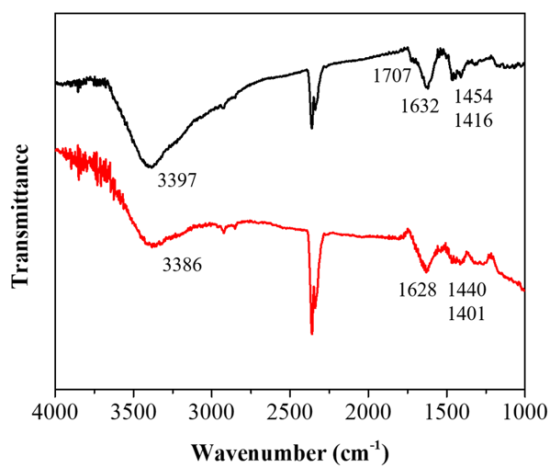Fig. S1. SEM images of DPIIF hydrogels at (a) 1 wt% and (b) 2 wt%. Scale bar: 100 nm.
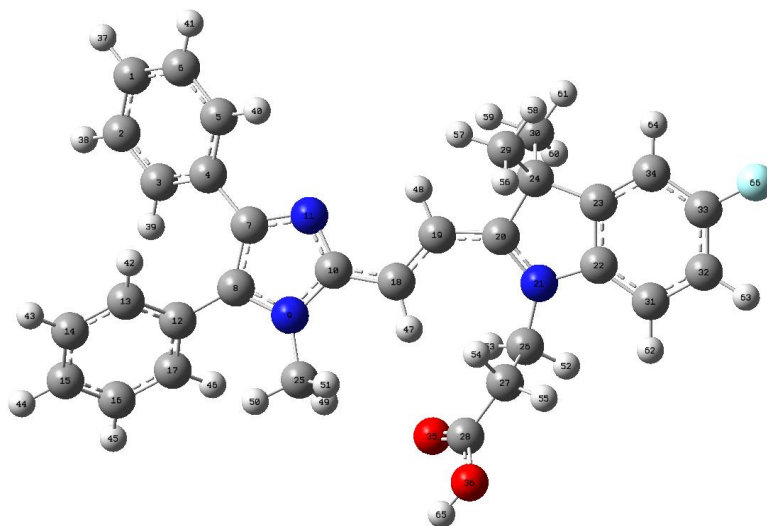

Fig. S2. FT-IR spectra of DPIIH (black) and DPIIF (red).

Table S2 NBO charge distribution of (*E*)-DPIIF, and (*Z*)-DPIIF by M06-2X/6-31G(d,p) level of theory using IEFPCM in water solvent.

(*E*)-DPIIF				(*Z*)-DPIIF			
C_1	-0.24743	C_{34}	-0.28954	C_1	-0.25154	C_{34}	-0.28751
C_2	-0.24665	O_{35}	-0.65335	C_2	-0.24622	O_{35}	-0.62269
C_3	-0.22893	O_{36}	-0.71815	C_3	-0.23174	O_{36}	-0.74771
C_4	-0.08859	H_{37}	0.2567	C_4	-0.08166	H_{37}	0.25586
C_5	-0.22414	H_{38}	0.25787	C_5	-0.22649	H_{38}	0.25679
C_6	-0.24728	H_{39}	0.25701	C_6	-0.24619	H_{39}	0.25596
C_7	0.13797	H_{40}	0.26027	C_7	0.12691	H_{40}	0.25175
C_8	0.19242	H_{41}	0.25744	C_8	0.16371	H_{41}	0.25589
N_9	-0.3375	H_{42}	0.26395	N_9	-0.34941	H_{42}	0.26277
C_{10}	0.32689	H_{43}	0.26245	C_{10}	0.34385	H_{43}	0.26138
N_{11}	-0.4786	H_{44}	0.26096	N_{11}	-0.52978	H_{44}	0.26003
C_{12}	-0.11583	H_{45}	0.26288	C_{12}	-0.11107	H_{45}	0.26172
C_{13}	-0.21544	H_{46}	0.26222	C_{13}	-0.21917	H_{46}	0.26068
C_{14}	-0.24256	H_{47}	0.25568	C_{14}	-0.24344	H_{47}	0.28365
C_{15}	-0.23593	H_{48}	0.28423	C_{15}	-0.23932	H_{48}	0.30172
C_{16}	-0.24205	H_{49}	0.26853	C_{16}	-0.24275	H_{49}	0.26248
C_{17}	-0.22956	H_{50}	0.2702	C_{17}	-0.23103	H_{50}	0.26996
C_{18}	-0.13456	H_{51}	0.26186	C_{18}	-0.20455	H_{51}	0.26207
C_{19}	-0.33212	B_{52}	0.28632	C_{19}	-0.31544	H_{52}	0.28924
C_{20}	0.39927	O_{53}	0.28401	C_{20}	0.46449	H_{53}	0.28933
N_{21}	0.31467	O_{54}	0.29615	N_{21}	0.27528	H_{54}	0.29125

C_{22}	0.13957	H_{55}	0.29447	C_{22}	0.1272	H_{55}	0.28811
C_{23}	-0.01567	H_{56}	0.26188	C_{23}	-0.01165	H_{56}	0.26364
C_{24}	-0.10613	H_{57}	0.25862	C_{24}	-0.11305	H_{57}	0.26081
C_{25}	-0.50044	H_{58}	0.26447	C_{25}	-0.5012	H_{58}	0.26871
C_{26}	-0.28235	H_{59}	0.25769	C_{26}	-0.27987	H_{59}	0.26153
C_{27}	-0.60727	H_{60}	0.26278	C_{27}	-0.59803	H_{60}	0.26335
C_{28}	0.87864	H_{61}	0.26554	C_{28}	0.87135	H_{61}	0.26537
C_{29}	-0.68425	H_{62}	0.279	C_{29}	-0.68537	H_{62}	0.28158
C_{30}	-0.68366	H_{63}	0.28378	C_{30}	-0.68388	H_{63}	0.28607
C_{31}	-0.23863	H_{64}	0.28442	C_{31}	-0.23483	H_{64}	0.28703
C_{32}	-0.29761	H_{65}	0.53804	C_{32}	-0.29702	H_{65}	0.53936
C_{33}	0.44281	F_{66}	-0.33805	C_{33}	0.4483	F_{66}	-0.33599

Table S3. Theoretically calculated electron transition energy of (*E*)-DPIIF using the TD-DFT/M06-2X/6-31G(d,p) level of theory with the PCM model in a water environment.
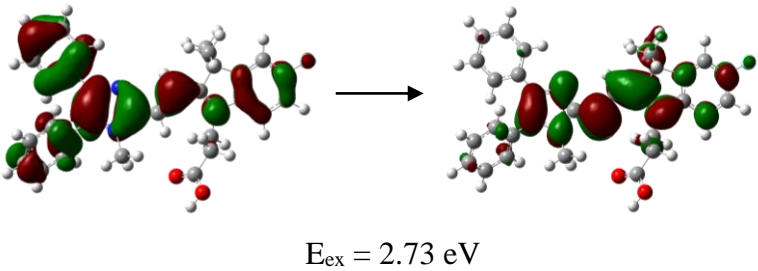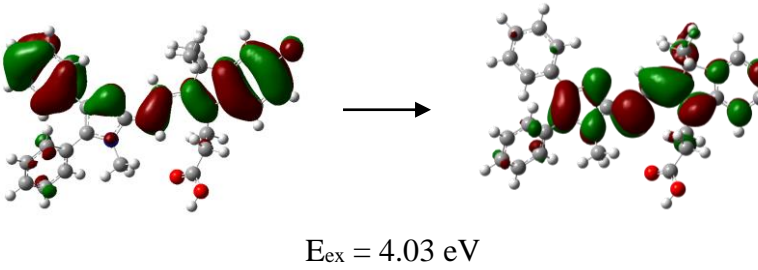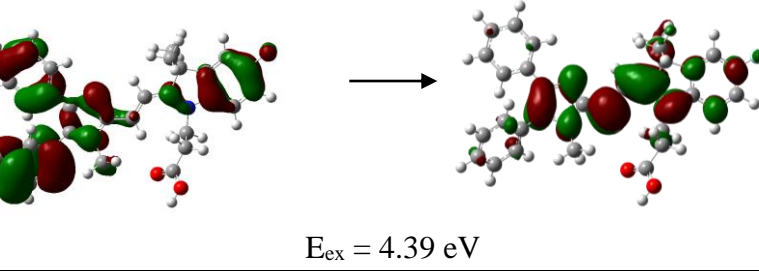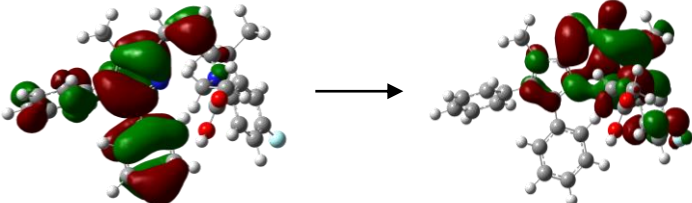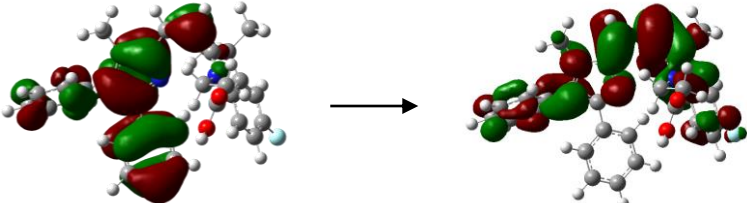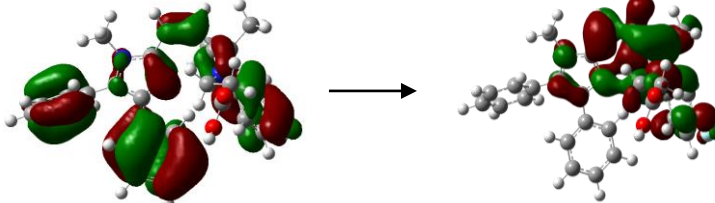
Bands (nm)	Electron transitions	Molecular orbitals
453.9	HOMO→LUMO Molecular contribution 0.69001 Oscillator strength (f) 1.3391	$E_{ex} = 2.73$ eV
307.7	HOMO-1→LUMO Molecular contribution 0.67705 Oscillator strength (f) 0.0606	$E_{ex} = 4.03$ eV
282.5	HOMO-3→LUMO Molecular contribution 0.55089 Oscillator strength (f) 0.0270	$E_{ex} = 4.39$ eV

Table S4. Theoretically calculated electron transition energy of (*Z*)-DPIIF using the TD-DFT/M06-2X/6-31G(d,p) level of theory with the PCM model in a water environment.
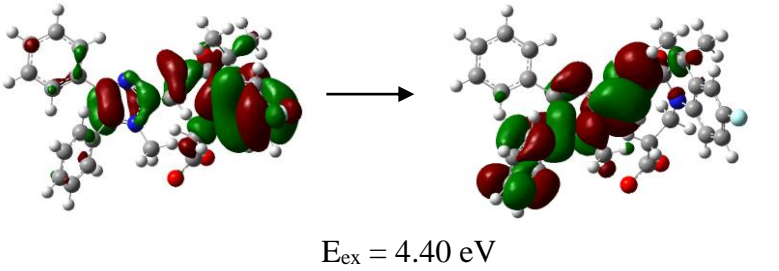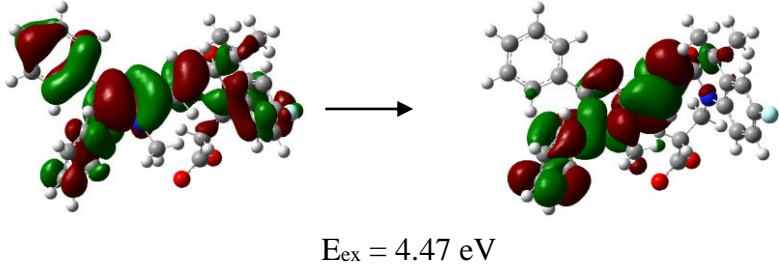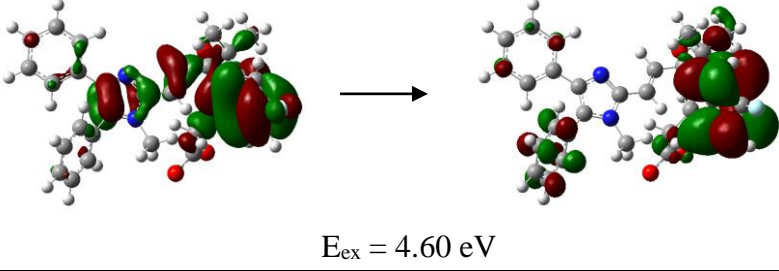
Bands (nm)	Electron transitions	Molecular orbitals
378.1	HOMO→LUMO Molecular contribution 0.67031 Oscillator strength (f) 0.2133	E_{ex} = 3.28 eV
280.9	HOMO→LUMO+1 Molecular contribution 0.57614 Oscillator strength (f) 0.3732	E_{ex} = 4.41 eV
274.9	HOMO-2→LUMO Molecular contribution 0.34858 Oscillator strength (f) 0.1649	E_{ex} = 4.51 eV

Table S5. Theoretically calculated electron transition energy of (*E*)-DPIIF-OH using the TD-DFT/M06-2X/6-31G(d,p) level of theory with the PCM model in a water environment.

Bands (nm)	Electron transitions	Molecular orbitals
281.5	HOMO→LUMO Molecular contribution 0.57564 Oscillator strength (f) 0.0743	$E_{ex} = 4.40$ eV
277.7	HOMO-1→LUMO Molecular contribution 0.61625 Oscillator strength (f) 0.6127	$E_{ex} = 4.47$ eV
269.4	HOMO→LUMO+2 Molecular contribution 0.42926 Oscillator strength (f) 0.2996	$E_{ex} = 4.60$ eV

Table S6. Theoretically calculated emission transition energy of (*E*)-DPIIF using the TD-DFT/M06-2X/6-31G(d,p) level of theory with the PCM model in a water environment.
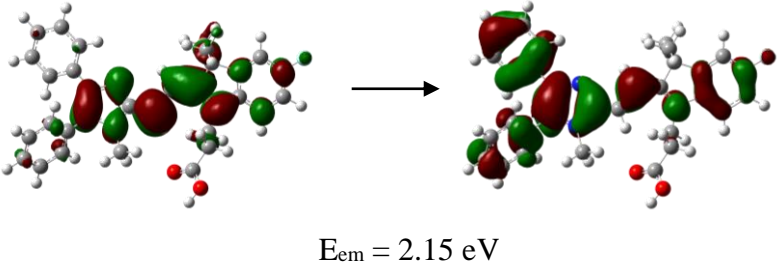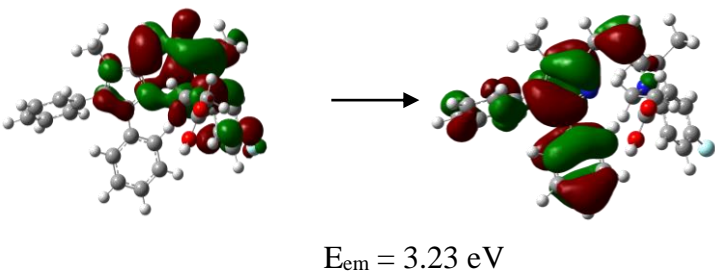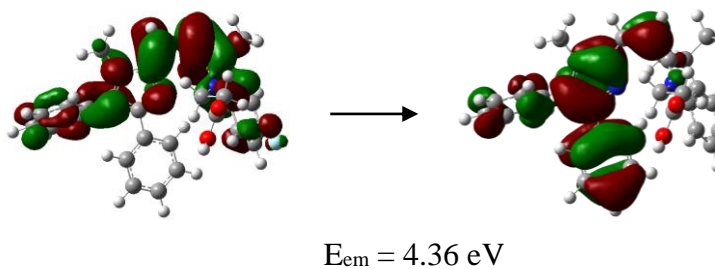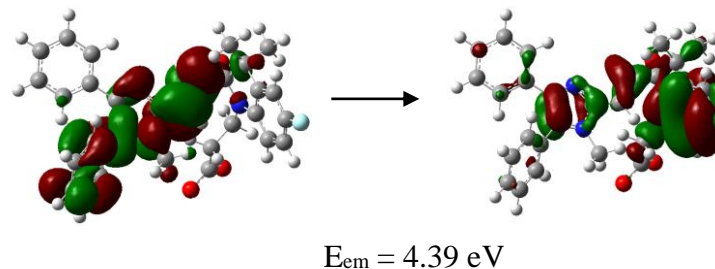
Bands (nm)	Electron transitions	Molecular orbitals
577.4	LUMO→HOMO Molecular contribution 0.69897 Oscillator strength (f) 1.0980	$E_{em} = 2.15$ eV

Table S7. Theoretically calculated emission transition energy of (*Z*)-DPIIF using the TD-DFT/M06-2X/6-31G(d,p) level of theory with the PCM model in a water environment.

Bands (nm)	Electron transitions	Molecular orbitals
384.03	LUMO→HOMO Molecular contribution 0.66861 Oscillator strength (f) 0.0761	$E_{em} = 3.23$ eV
284.41	LUMO+1→HOMO Molecular contribution 0.63782 Oscillator strength (f) 0.1843	$E_{em} = 4.36$ eV

Table S8. Theoretically calculated emission transition energy of (*E*)-DPIIF-OH using the TD-DFT/M06-2X/6-31G(d,p) level of theory with the PCM model in a water environment.

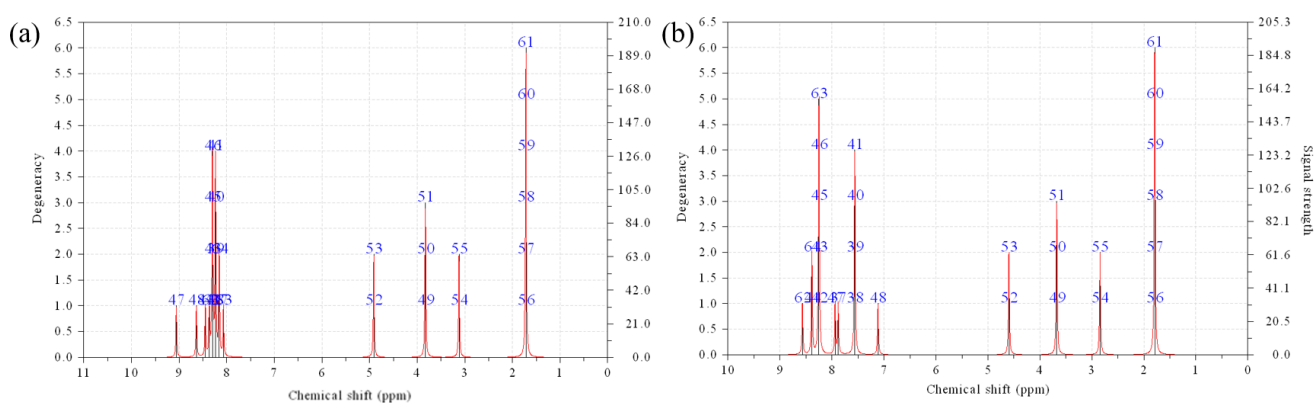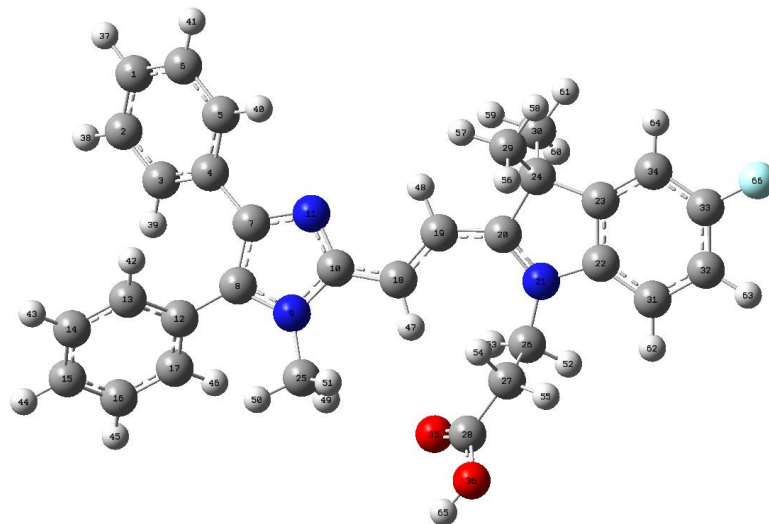| Bands (nm)	Electron transitions	Molecular orbitals
282.19	LUMO→HOMO Molecular contribution 0.60623 Oscillator strength (f) 0.2095	$E_{em} = 4.39$ eV

Fig. S3. Theoretical ^{1}H NMR spectra of (a) (*E*)-DPIIF and (b) (*Z*)-DPIIF by the DFT/M06-2X/6-31G(d,p) level of theory with PCM model in a DMSO environment.

Table S9. Theoretical ^{1}H NMR calculations for (*E*)-DPIIF and (*Z*)-DPIIF by the DFT/M06-2X/6-31G(d,p) level of theory with PCM model in a DMSO environment.

(*E*)-DPIIF Atom	Chemical Shift (ppm)	(*Z*)-DPIIF Atom	Chemical Shift (ppm)
H_{56}、H_{57}、H_{58}、H_{59}、H_{60}、H_{61}	1.72	H_{56}、H_{57}、H_{58}、H_{59}、H_{60}、H_{61}	1.79
H_{54}、H_{55}	3.12	H_{54}、H_{55}	2.84
H_{49}、H_{50}、H_{51}	3.83	H_{49}、H_{50}、H_{51}	3.68
H_{52}、H_{53}	4.91	H_{52}、H_{53}	4.60
H_{63}	8.07	H_{48}	7.11
H_{37}、H_{64}	8.16	H_{38}、H_{39}、H_{40}、H_{41}	7.56
H_{38}、H_{39}、H_{40}、H_{41}	8.24	H_{37}	7.88
H_{42}、H_{43}、H_{45}、H_{46}	8.30	H_{47}	7.94
H_{62}	8.37	H_{42}、H_{43}、H_{45}、H_{46}、H_{63}	8.25
H_{44}	8.45	H_{44}、H_{64}	8.39
H_{48}	8.64	H_{62}	8.57
H_{47}	9.06		

Table S10. Comparison of theoretical and experimental chemical shifts of H47 (Ha) and H48 (Hb) in ^{1}H NMR for (E)-DPIIF and (Z)-DPIIF.[a]

(E)-DPIIF Atom	Chemical Shift (ppm)	(Z)-DPIIF Atom	Chemical Shift (ppm)
H47[b]	9.06	H47[b]	7.94
H48[b]	8.64	H48[b]	7.11
Ha[c]	8.09	Ha[c]	6.92
Hb[c]	7.83	Hb[c]	6.75

[a]H47 represents Ha, and H48 represents Hb. [b]theoretical chemical shifts, [c]experimental chemical shifts.
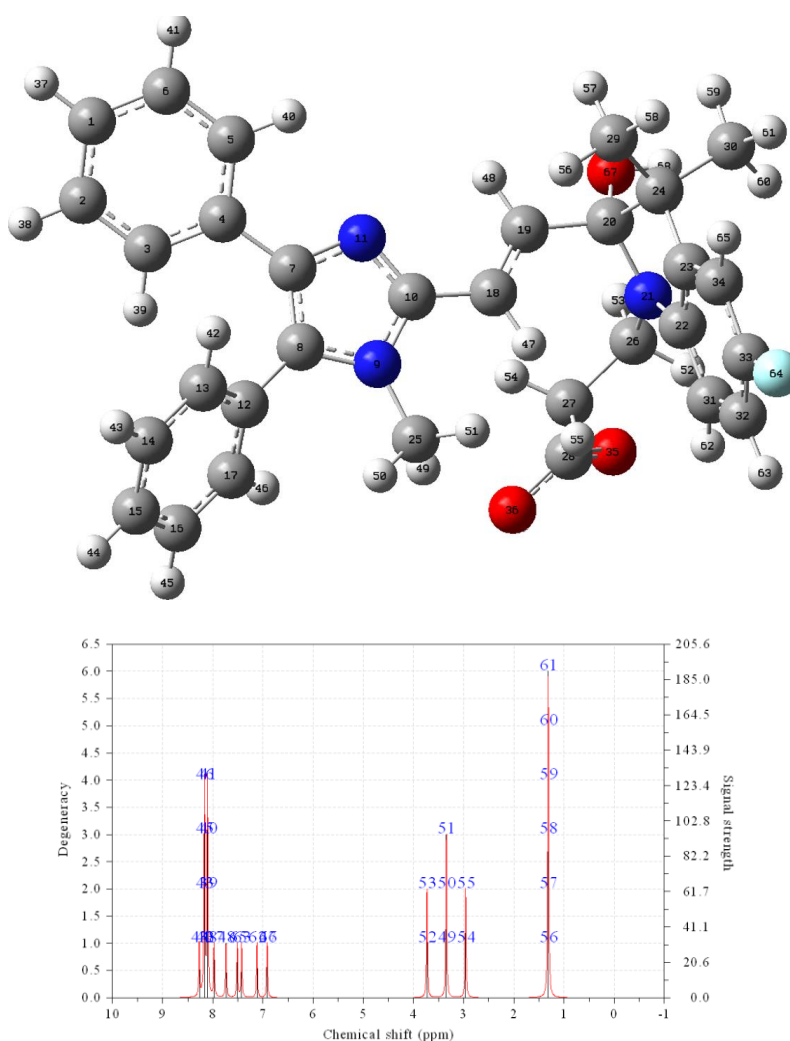

Fig. S4. Theoretical ^{1}H NMR spectrum of (E)-DPIIF-OH by the DFT/M06-2X/6-31G(d,p) level of theory with PCM model in a DMSO environment.

Table S11. Theoretical ^{1}H NMR calculations for (*E*)-DPIIF-OH by the DFT/M06-2X/6-31G(d,p) level of theory with PCM model in a DMSO environment.

Atom	Chemical Shift (ppm)
H$_{56}$、H$_{57}$、H$_{58}$、H$_{59}$、H$_{60}$、H$_{61}$	1.31
H$_{54}$、H$_{55}$	2.96
H$_{49}$、H$_{50}$、H$_{51}$	3.34
H$_{52}$、H$_{53}$	3.73
H$_{47}$	6.92
H$_{62}$	7.12
H$_{63}$	7.42
H$_{48}$	7.51
H$_{65}$	7.74
H$_{37}$	7.97
H$_{38}$、H$_{39}$、H$_{40}$、H$_{41}$	8.10
H$_{42}$、H$_{43}$、H$_{45}$、H$_{46}$	8.17
H$_{44}$	8.27

Table S12. Comparison of theoretical and experimental chemical shifts of H$_{47}$ (H$_a$) and H$_{48}$ (H$_b$) in ^{1}H NMR for (*E*)-DPIIF-OH.[a]

Atom	Chemical Shift (ppm)
H$_{47}$[b]	6.92
H$_{48}$[b]	7.51
H$_a$[c]	6.62
H$_b$[c]	6.88

[a]H$_{47}$ represents H$_a$, and H$_{48}$ represents H$_b$. [b]theoretical chemical shifts, [c]experimental chemical shifts.

Table S13. The quantum yields of DPIIF in solution and solid state.

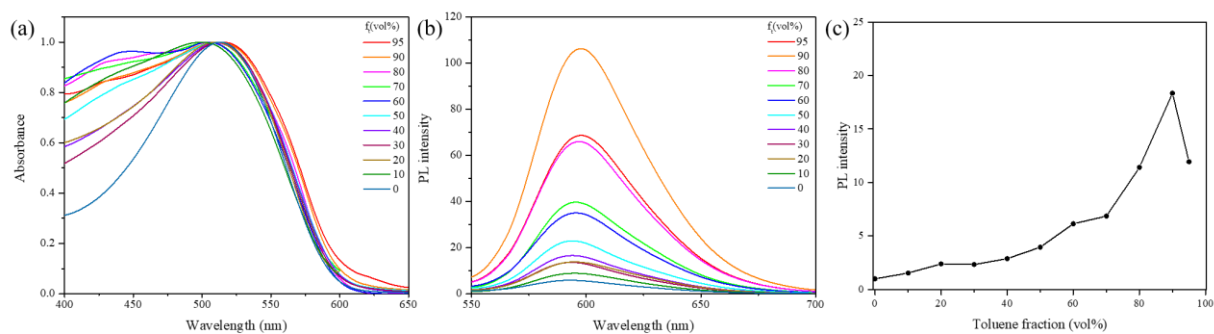| Solution[a,b]	Solid[b]
1.82%	9.05%

[a]Measured in DMSO; [b]Determined by absolute method.[S19]

Fig. S5. (a) UV-vis absorption and (b) emission spectra of DPIIF at 5 µM in toluene/DMSO mixtures (λex= 513.8). (c) Plot of the relative fluorescence intensity (I/I_0) of DPIIF with respect to the fraction of toluene in the toluene/DMSO mixtures; I_0: fluorescence intensity at 598 nm in pure DMSO.
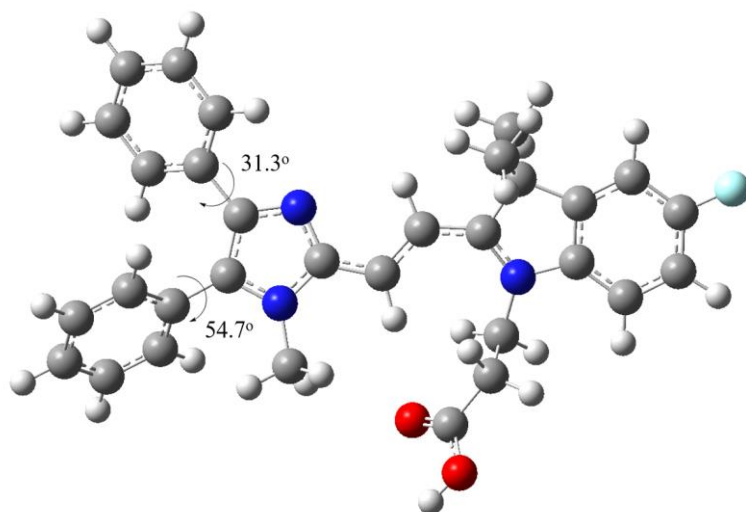

Fig. S6. (*E*)-DPIIF was optimized using the DFT/M06-2X/6-31G(d,p) level of theory with the PCM solvation model (water as the solvent). Carbon, hydrogen, nitrogen, oxygen, and fluorine atoms are depicted in gray, white, blue, red, and cyan, respectively.

H$_2$O-H$_2$O

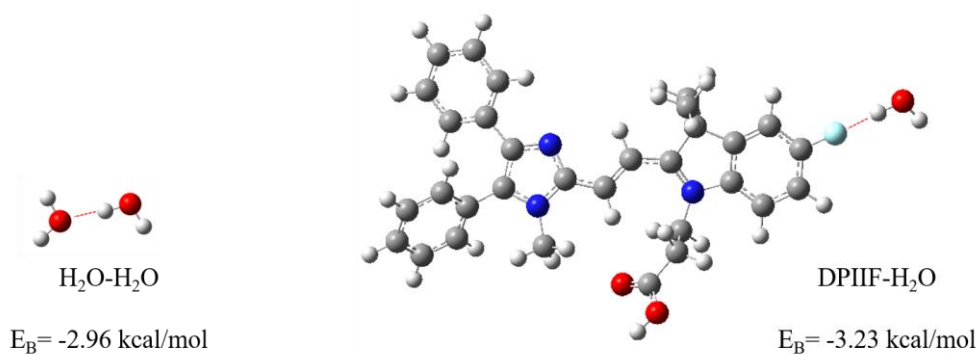E$_B$= -2.96 kcal/mol

DPIIF-H$_2$O

E$_B$= -3.23 kcal/mol

Fig. S7. DFT analysis of the intermolecular binding energy between DPIIF and water. Carbon, hydrogen, nitrogen, oxygen, and fluorine atoms are depicted in gray, white, blue, red, and cyan, respectively.
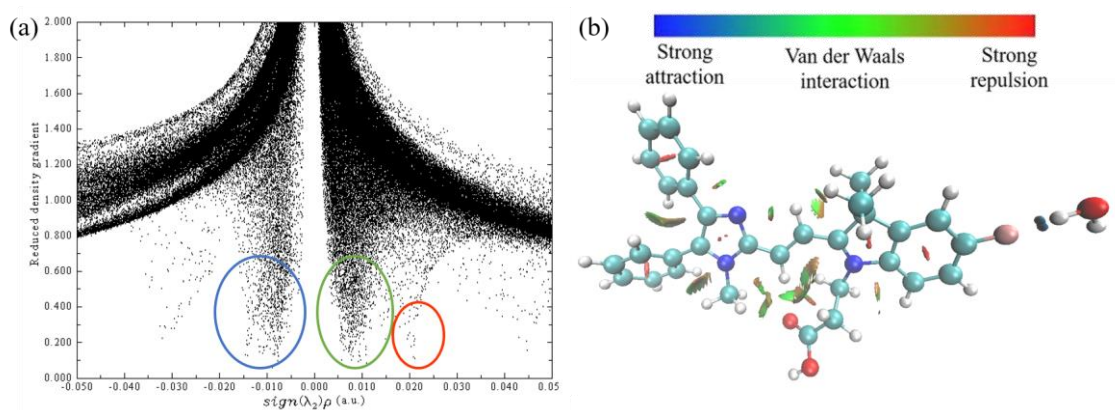

Fig. S8. Reduced density gradient (σ) between DPIIF and water, plotted with respect to the electron density (ρ) multiplied by the sign of λ$_2$. (b) Visualization of the intermolecular interactions between DPIIF and water in real space; carbon, hydrogen, nitrogen, oxygen, and fluorine atoms are depicted in cyan, white, blue, red, and pink, respectively.
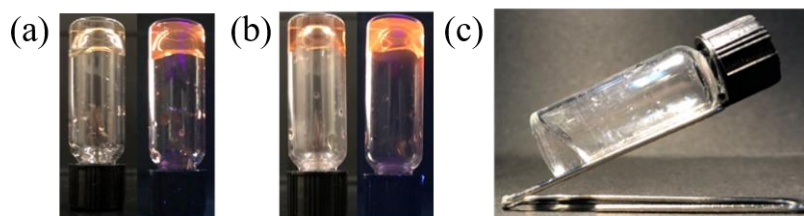
Fig. S9. Optical images of 1 wt% (*E*)-DPIIF at (a) pH 2, (b) pH 7, and (c) pH 12, with (a) and (b) captured under ambient room lighting (left) and UV illumination (right).
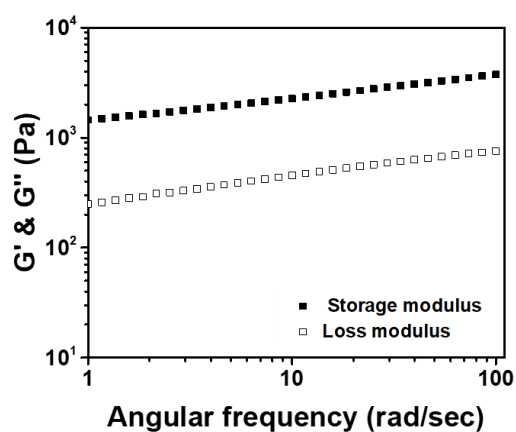

Fig. S10. Frequency-dependent rheology measurement of 2 wt% of (*E*)-DPIIF hydrogel.
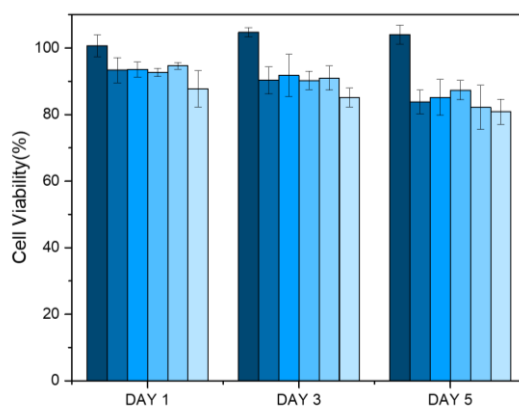

Fig. S11. Cell viability of L929 cells on DPIIF hydrogels for 1, 3, and 5 days. (From left to right are the control, pH 5.5, pH 6.5, pH 7.0, pH 8.0, and samples exposed to UV light irradiation for 30 seconds.)
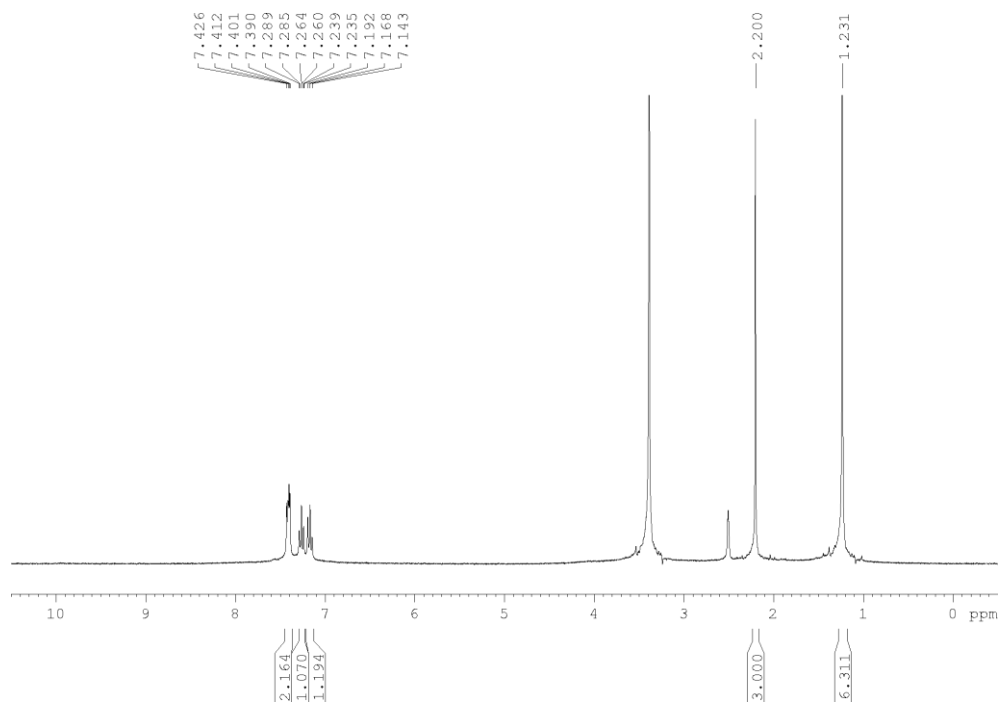
Fig. S12. ^{1}H NMR spectrum of compound **5a** in DMSO-d_6.
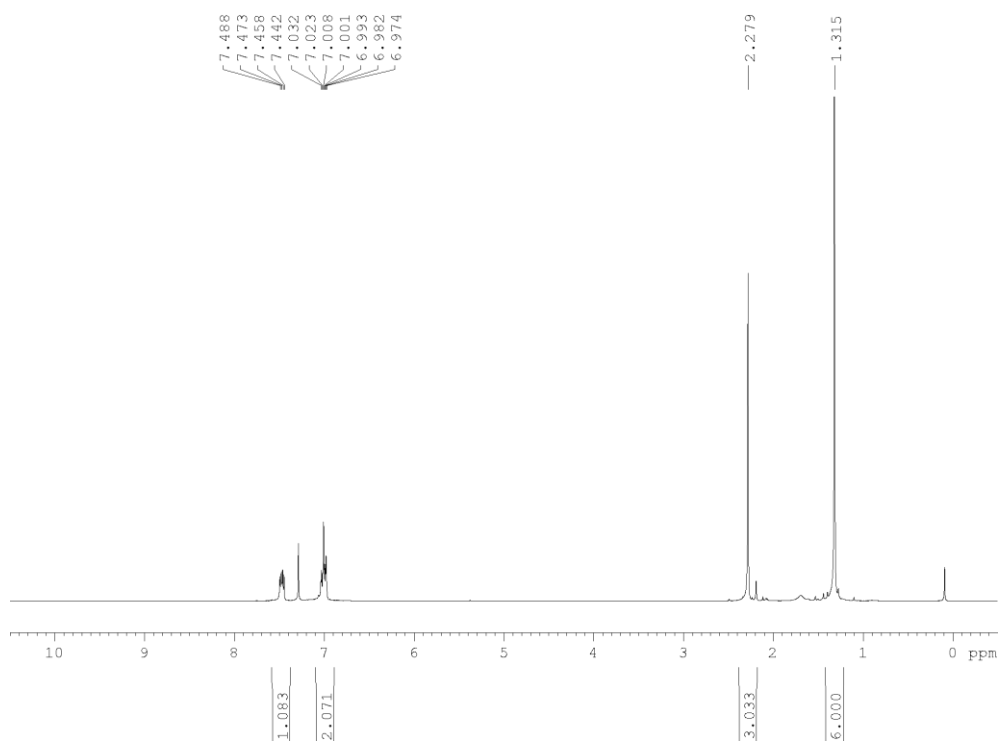
Fig. S13. ^{1}H NMR spectrum of compound **5b** in CDCl$_3$.

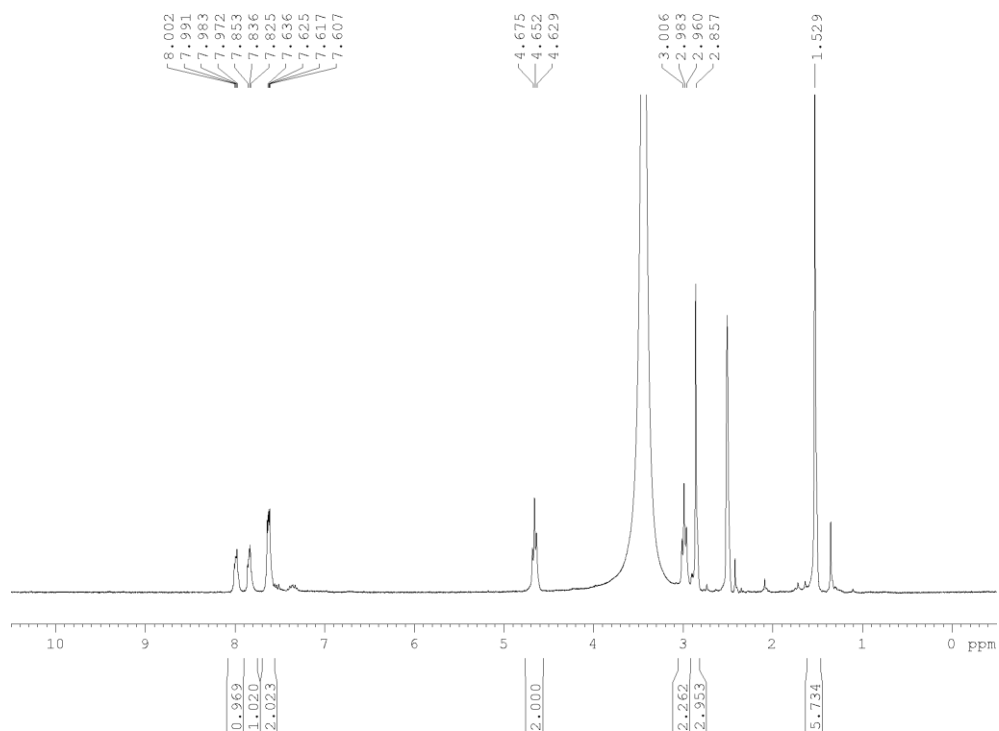Fig. S14. ¹H NMR spectrum of compound **6a** in DMSO-*d₆*.
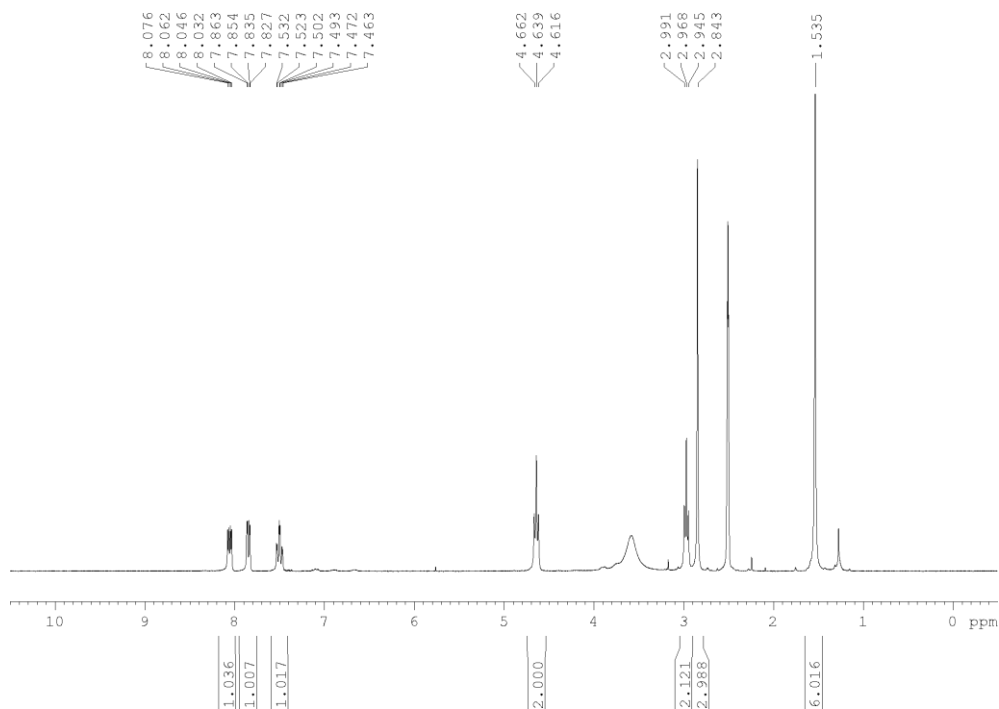
Fig. S15. ¹H NMR spectrum of compound **6b** in DMSO-*d₆*.
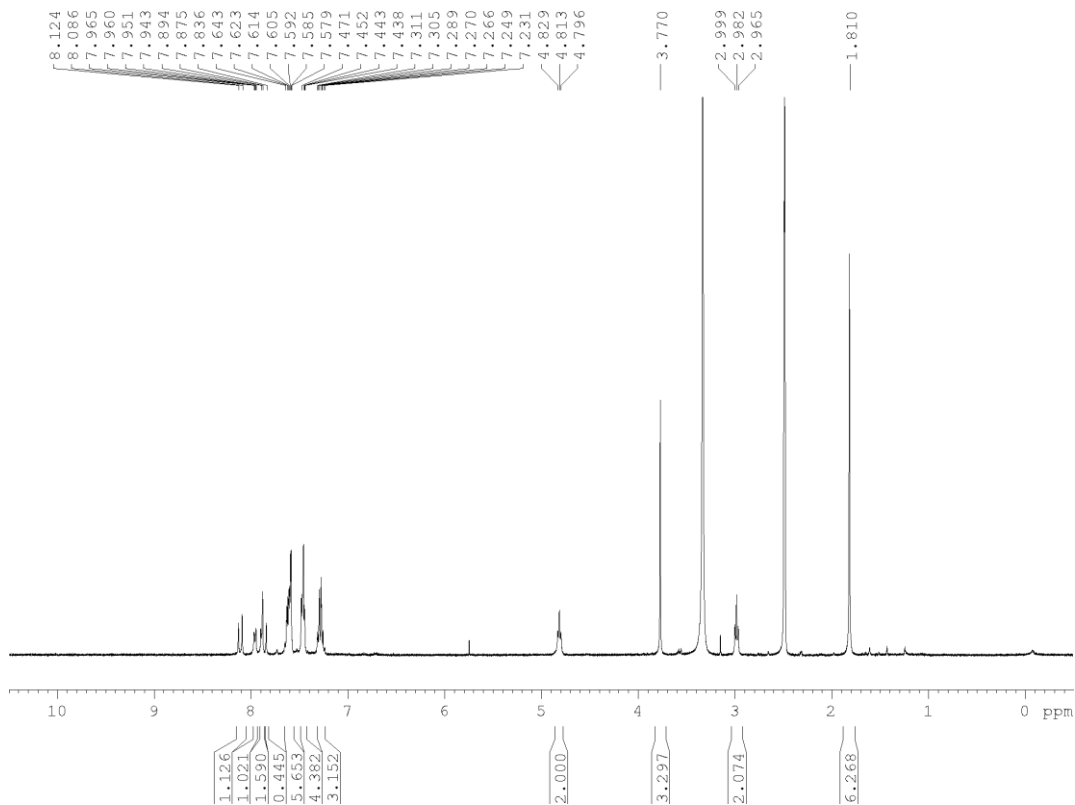
Fig. S16. ¹H NMR spectrum of DPIIH in DMSO-*d₆*.
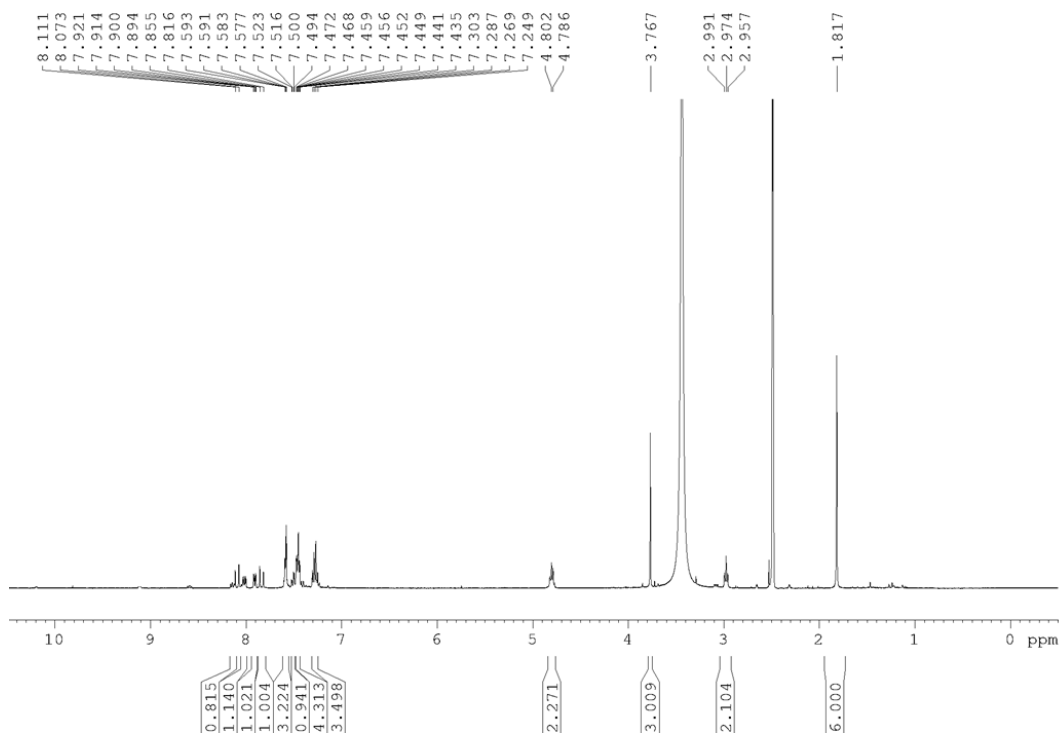

Fig. S17. ¹H NMR spectrum of DPIIF in DMSO-*d₆*.

Data:Im H
Comment:
Description:
Ionization Mode:ESI+
History:Average(MS[1] 0.21..0.48)

Acquired:4/15/2024 3:45:30 PM
Operator:AccuTOF
m/z Calibration File:20240411-TFANa_...
Created:4/17/2024 11:33:43 AM
Created by:AccuTOF

Charge number:1
Element:^{12}C:31 .. 31, ^{1}H:15 .. 31, ^{14}N:3 .. 3, ^{23}Na:0 .. 2, ^{16}O:2 .. 2

Tolerance:400.00[ppm], 400.00 .. 400....

Unsaturation Number:-300.5 .. 300.0 (...

Relative Intensity

60

40

476.25933

20

504.29552

427.35569 451.01755   527.79500   571.03945   615.26482   654.63880

0

450   500   550   600   650
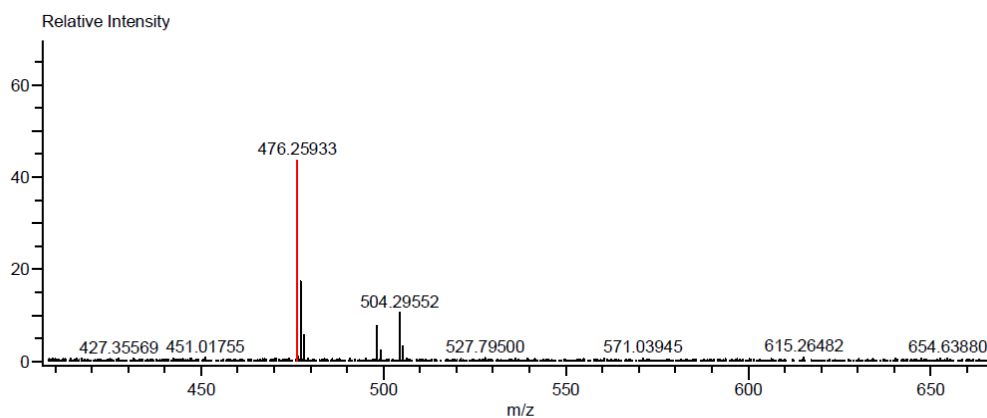
m/z

Fig. S18. HRMS spectrum of DPIIH.

Data:Im F
Comment:
Description:
Ionization Mode:ESI+
History:Average(MS[1] 0.25..0.39)

Acquired:4/15/2024 3:48:34 PM
Operator:AccuTOF
m/z Calibration File:20240411-TFANa_...
Created:4/17/2024 11:32:19 AM
Created by:AccuTOF

Charge number:1
Element:^{12}C:31 .. 31, ^{1}H:15 .. 31, ^{14}N:3 .. 3, ^{23}Na:0 .. 2, ^{16}O:2 .. 2

Tolerance:400.00[ppm], 400.00 .. 400....

Unsaturation Number:-300.5 .. 300.0 (...

Relative Intensity

40

494.24692

20

522.27878

668.34885

692.35702

446.23034 471.91436   544.52121   575.29925   608.80921   639.88713

0

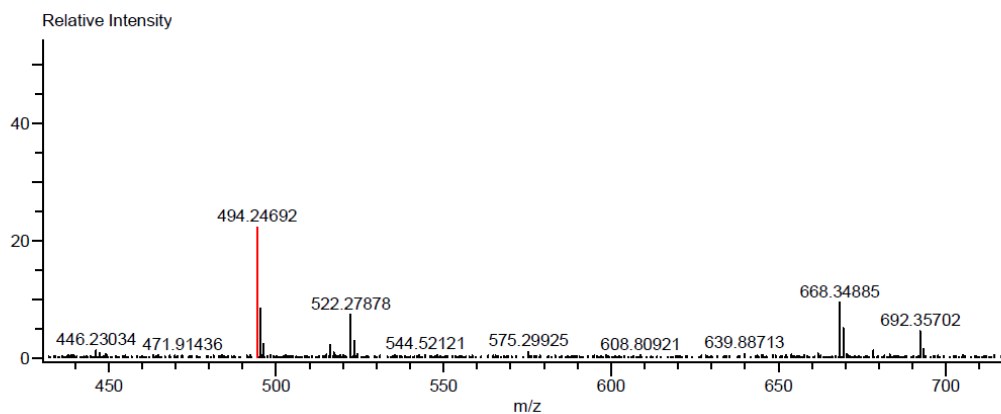450   500   550   600   650   700

m/z

Fig. S19. HRMS spectrum of DPIIF.

Reference

S1. A. O. Okaru, T. S. Brunner, S. M. Ackermann, T. Kuballa, S. G. Walch, M. Kohl-Himmelseher, D. W. Lachenmeier, *J. Anal. Methods Chem.* **2017**, *2017*, 9206297.

S2. Y.-S. Zhang, X.-J. Liu, Y.-Z. Chu, P.-W. Chen, Y.-C. Yeh, Y.-F. Ni, M.-Y. Yeh, *ACS Appl. Electron. Mater.* **2023**, *5*, 6114.

S3. H.-Y. Chen, C.-C. Yao, T.-Y. Tseng, Y.-C. Yeh, H.-S. Huang, M.-Y. Yeh, *RSC Adv.* **2021**, *11*, 40228.

S4. M.-Y. Yeh, C.-T. Huang, T.-S. Lai, F.-Y. Chen, N.-T. Chu, D. T.-H. Tseng, S.-C. Hung, H.-C. Lin, *Langmuir* **2016**, *32*, 7630.

S5. ISO 10993-5: 2009 Biological Evaluation of Medical Devices-Part 5: Tests for in Vitro Cytotoxicity (International Organization for Standardization, **2009**).

S6. C. R. Kruse, M. Singh, S. Targosinski, I. Sinha, J. A. Sorensen, E. Eriksson, K. Nuutila, *Wound Rep. Reg.* **2017**, *25*, 260-269.

S7. A. Souza, M. Parnell, B. J. Rodriguez, E. G. Reynaud, *Gels* **2023**, *9*, 853.

S8. Y. Zheng, H. Lu, Z. Jiang, Y. Guan, J. Zou, X. Wang, R. Cheng, H. Gao, *J. Mater. Chem. B*, **2017**, *5*, 6277-6281.

S9. M. J. Frisch et al., Gaussian 09 ,Revision D.01, Gaussian Inc., Wallingford CT, **2009**.

S10. H. Wang, Q. Li, J. Zhang, H. Zhang, Y. Shu, Z. Zhao, W. Jiang, L. Du, D. L. Phillips, J. W. Y. Lam, H. H. Y. Sung, I. D. Williams, R. Lu and B. Z. Tang, *J. Am. Chem. Soc.* **2021**, *143*, 9468.

S11. B. J. Graham, I. W. Windsor, B. Gold, R. T. Raines, *Proc. Natl. Acad. Sci. USA* **2021**, *118*, e2013691118.

S12. Y. Zhao, D. G. Truhlar, *Theor. Chem. Acc.* **2008**, *120*, 215.

S13. M.-Y. Yeh, H.-C. Lin, *Phys. Chem. Chem. Phys.* **2014**, *16*, 24216.

S14. B. Mennucci, E. Cances, J. Tomasi, *J. Phys. Chem. B* **1997**, *101*, 10506.

S15. K. Wolinski, J. F. Hinton, P. Pulay, *J. Am. Chem. Soc.* **1990**, *112*, 8251.

S16. S. F. Boys and F. Bernardi, *Mol. Phys.*, **1970**, *19*, 553-566.

S17. T. Lu and F. Chen, *J. Comput. Chem.*, **2012**, *33*, 580-592.

S18. E. R. Johnson, S. Keinan, P. Mori-Sánchez, J. Contreras-García, A. J. Cohen and W. Yang, *J. Am. Chem. Soc.*, **2010**, *132*, 6498-6506

S19. Z. Song, W. Zhang, M. Jiang, H. H. Y. Sung, R. T. K. Kwok, H. Nie, I. D. Williams, B. Liu, B. Z. Tang, *Adv. Funct. Mater.* **2016**, *26*, 824.